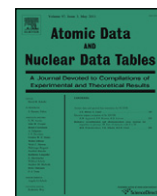




Contents lists available at SciVerse ScienceDirect

Atomic Data and Nuclear Data Tables

journal homepage: www.elsevier.com/locate/adt

Photoionization and photoabsorption cross sections for the aluminum iso-nuclear sequence

M.C. Witthoef^{a,b,*}, M.A. Bautista^c, J. García^{b,c}, T.R. Kallman^b, C. Mendoza^d, P. Palmeri^e, P. Quinet^{e,f}

^a Department of Astronomy, University of Maryland, College Park, MD, USA

^b NASA/Goddard Space Flight Center, Code 662, Greenbelt, MD, USA

^c Department of Physics, Western Michigan University, Kalamazoo, MI, USA

^d Centro de Física, Instituto Venezolano de Investigaciones Científicas (IVIC), Caracas, Venezuela

^e Astrophysique et Spectroscopie, Université de Mons - UMONS, B-7000 Mons, Belgium

^f INPAS, Université de Liège, B-4000 Liège, Belgium

ARTICLE INFO

Article history:

Received 8 September 2011

Received in revised form

11 January 2012

Accepted 9 April 2012

Available online 29 December 2012

ABSTRACT

K-shell photoionization and photoabsorption cross sections are presented for Li-like to Na-like Al. The calculations are performed using the Breit–Pauli *R*-matrix method where the effects of radiation and Auger dampings are included. We provide electronic data files for the raw cross sections as well as those convolved with a Gaussian of width $\Delta E/E = 10^{-4}$. In addition to total cross sections for photoabsorption and photoionization, partial cross sections are available for photoionization.

© 2012 Elsevier Inc. All rights reserved.

* Corresponding author at: Department of Astronomy, University of Maryland, College Park, MD, USA.
E-mail address: michael.c.witthoef@nasa.gov (M.C. Witthoef).

Contents

1. Introduction.....	54
2. Numerical methods.....	54
3. Results.....	54
4. Conclusions.....	57
Acknowledgments	57
Appendix. Supplementary data.....	57
References.....	58
Explanation of Table	59

1. Introduction

This work is a continuation of a program to calculate K-shell atomic data for all ions of astrophysical importance. Our previous work on other ions includes the iso-nuclear sequences: N [1]; O [2]; Ne, Mg, Si, S, Ar, and Ca [3–5]; Fe [6–11]; and Ni [12,13]. In this paper, we report on photoabsorption and photoionization cross sections for the Li-like to Na-like ions of Al calculated using the Breit-Pauli *R*-matrix method. This data complements the energy levels, Einstein *A* coefficients, and Auger rates computed by Palmeri et al. [14].

While Aluminum K lines tend to be weak in X-ray spectra, the current fleet of X-ray satellite telescopes (Chandra, XMM Newton, and Suzaku) are sensitive enough to observe them. Most observations of Al to date have been from the H- and He-like stages; see Ref. [14] for a summary. We expect that the data presented here will lead to more identifications from other Al ions in the future.

There are few previous calculations mapping out the resonance structure near the K edge of Al ions. We are aware of two such calculations for the Li-like [15] and N-like [16] ions. Calculations and measurements of the background cross sections are also scarce; see the compilations and fitting performed by Veigele [17] and Verner and Yakovlev [18]. Work on valence-shell photoionization, however, is more abundant. *R*-matrix calculations for various ions have been performed by the Opacity Project [19–23], as well as others [24–27].

2. Numerical methods

The photoionization calculations are performed using the Breit-Pauli *R*-matrix method [28], which has a long history of development [29–32]. For inner-shell processes, radiative decay and the spectator Auger process can affect the size and shape of resonance features. These effects, known as radiation and Auger damping [33], are included in the *R*-matrix calculations [34,35] by introducing an imaginary component to the resonance energies which is equal to the sum of the radiative and Auger widths. The inclusion of damping causes the absorption and ionization cross sections to differ since not every incident photon will result in a photo-electron. We use the *R*-matrix computer package of Berrington et al. [36] for the inner region calculation and the asymptotic region code, STGBFODAMP¹ [34], is used to compute the photoabsorption and photoionization cross sections including the effects of damping.

The target expansion for the Li-like to Ne-like ions includes all levels of the configurations: $1s^2 2l^w$ and $1s 2l^{w+1}$ where $w = 0$ for Li-like and $w = 7$ for Ne-like. Note that the target refers to the final state which has one fewer electron than the initial state; thus the Ne-like case having an 9-electron target. For the Na-like system, we include the configurations $1s^2 2l^8$, $1s^2 2l^7 3l$, $1s^2 2l^7 3d$, and $1s 2l^8 3l$ where l is restricted to s- and p-electrons.

The atomic orbitals used in the *R*-matrix calculations are obtained using AUTOSTRUCTURE [37,38] where Thomas–Fermi–Amaldi

scaling factors are optimized on the lowest average energy of all states. In the *R*-matrix calculations, the level energies are adjusted during diagonalization of the Hamiltonian to match those listed at NIST [39] or recent relativistic Hartree–Fock calculations [14]. The ionization threshold of the cross sections are also shifted to match data from NIST. This shift brings the K edge positions in agreement with the values in the work of Palmeri et al. [14] due to the matching of energy levels mentioned above.

It is important to include enough continuum basis orbitals in the calculations to accurately represent the photo-electrons. The general rule of thumb is for the continuum basis orbitals to span twice the desired maximum energy of the outgoing electron. If too few are included, oscillations in the cross section will be seen at high energies followed by a rapid drop-off once the energy of the final continuum basis function is exceeded. Using this rule of thumb for the Li-like to F-like ions, we include enough continuum basis orbitals to span twice the position of the K edge; between 20 and 25 basic orbitals were needed. For Ne-like Al, weak oscillations were found in the cross sections below the K edge. To remove these oscillations, we increased the size of the *R*-matrix radius beyond the default value chosen by the codes (from 3.2 to 6.0). The larger box size also required a set of 50 continuum basis orbitals per angular momentum. For the Na-like calculation, 60 continuum basis orbitals were used to allow for accurate cross sections up to at least 1.5 times the K edge energy.

These calculations were performed on the NCCS Discover cluster at NASA/Goddard Space Flight Center. Typically 16 processors are needed for the inner region while up to 64 processors were used for the outer region calculation.

3. Results

The photoionization results reproduce the same overall features as seen in our previous calculations for other ions. In Figs. 1–9, we show the photoabsorption and photoionization cross sections for Li-like to Na-like Al using the same scales for the energy and cross section axes in each figure. The magnitude of the background cross sections, both above and below the K edge, does not change much along the isonuclear sequence since the $1s$ wavefunction is little affected by the addition of electrons to the outer subshells. The location of the edge and resonance structure, however, is dependent on the structure of each specific ion. As the number of electrons increases, the K edge moves to lower photon energies (from about 2 keV for Li-like Al to 1.6 keV for the Na-like ion). Also, the spread of the resonances in energy is decreased; the Li-like resonances span about 0.5 keV while, for Na-like Al, all K resonances are contained within 0.1 keV of the edge.

The strength of damping in the photoionization cross sections increases as the photon energy approaches the K edge. At the K edge, the photoionization resonances are nearly damped away entirely. This does not mean, however, that these resonances do not lead to a photo-electron. The difference between the photoabsorption and photoionization cross sections is the probability of either radiative stabilization or a spectator Auger process. It is only the participator Auger process that is being ‘damped’. The radiative and

¹ <http://amdpp.phys.strath.ac.uk/tamoc/code.html>.

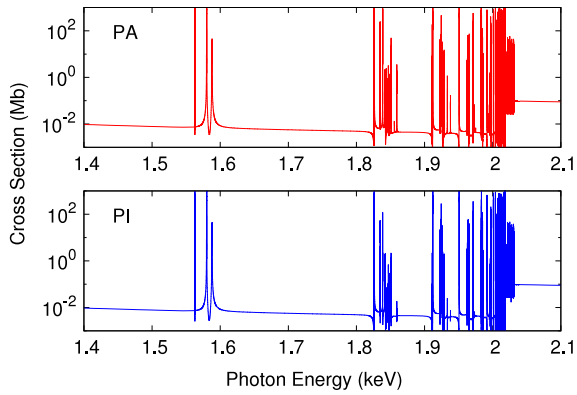


Fig. 1. Total photoabsorption (top) and photoionization (bottom) cross sections of Li-like Al.

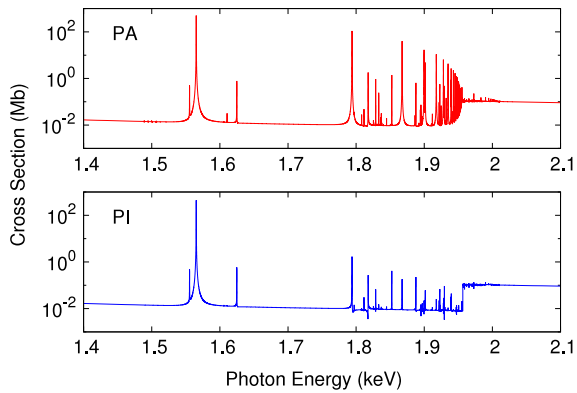


Fig. 2. Total photoabsorption (top) and photoionization (bottom) cross sections of Be-like Al. The photoionization cross section does not include the effect of spectator Auger loss.

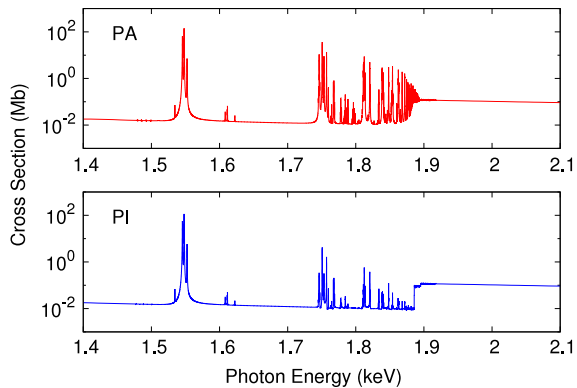


Fig. 3. Total photoabsorption (top) and photoionization (bottom) cross sections of B-like Al. The photoionization cross section does not include the effect of spectator Auger loss.

Auger yields of the core states can give an estimate of how much of the damped cross section goes to either process; see the work of Palmeri et al. [14] for the yields. In fact, the majority of the photoabsorption ultimately leads to an ionization process.

As the charge state decreases from Li-like to Ne-like, we begin to observe small oscillations in the background cross section below the K edge. Prior to increasing the R -matrix box size, the largest oscillations were for the Ne-like ion which varied the cross section about the mean by at most 10%, which is the expected level of uncertainty for these calculations. Nearly doubling the R -matrix radius completely removed the oscillations without changing the mean background cross section nor the positions of the resonance

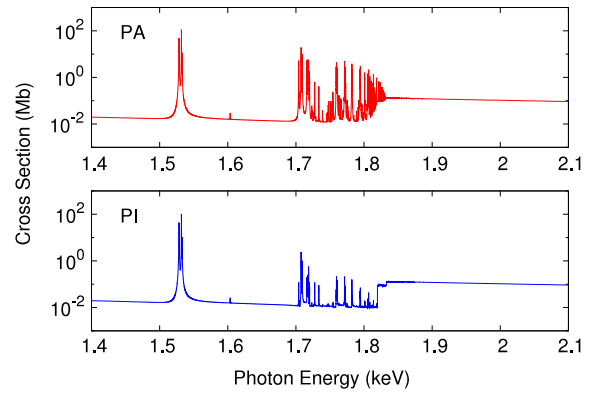


Fig. 4. Total photoabsorption (top) and photoionization (bottom) cross sections of C-like Al. The photoionization cross section does not include the effect of spectator Auger loss.

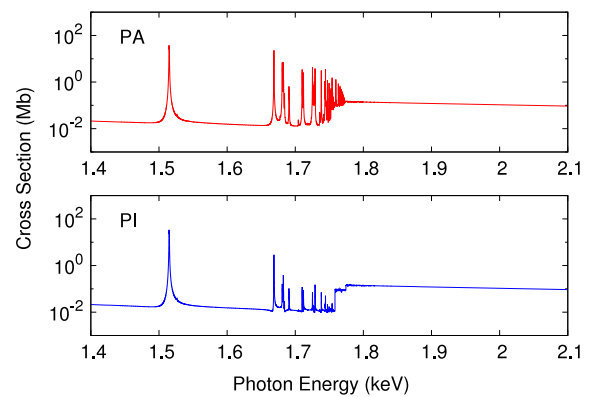


Fig. 5. Total photoabsorption (top) and photoionization (bottom) cross sections of N-like Al. The photoionization cross section does not include the effect of spectator Auger loss.

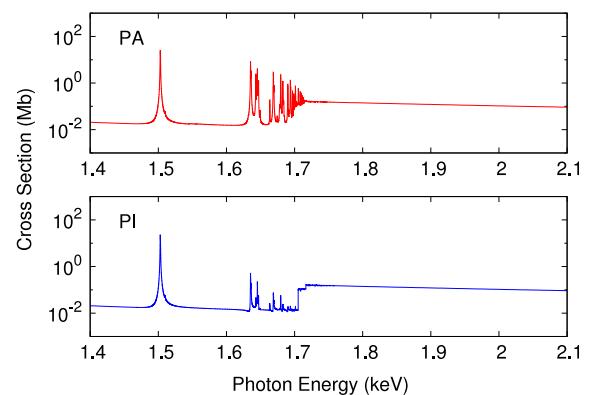


Fig. 6. Total photoabsorption (top) and photoionization (bottom) cross sections of O-like Al. The photoionization cross section does not include the effect of spectator Auger loss.

features. The oscillations are negligible for the other ions when using the default R -matrix radius.

To our knowledge, the only previous calculations for K-shell photoionization which include the resonance contribution for the Al ions covered in this work are by Nahar [15] for Li-like Al and Zeng et al. [16] for N-like Al. Other measurements and calculations for photoionization of Al ions which do not include the resonant contribution are summarized and fit by Verner and Yakovlev [18]. The K edge positions in that work are typically 15–30 eV lower than those given by Palmeri et al. [14]. Once the cross sections are shifted to bring the K edge positions into agreement, the

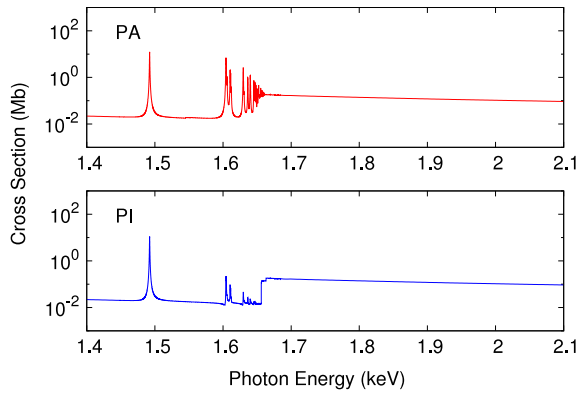


Fig. 7. Total photoabsorption (top) and photoionization (bottom) cross sections of F-like Al. The photoionization cross section does not include the effect of spectator Auger loss.

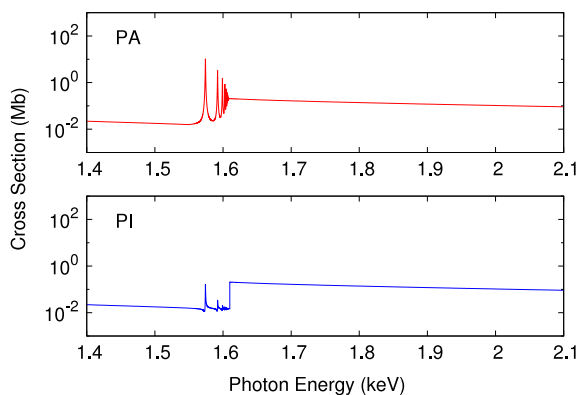


Fig. 8. Total photoabsorption (top) and photoionization (bottom) cross sections of Ne-like Al. The photoionization cross section does not include the effect of spectator Auger loss.

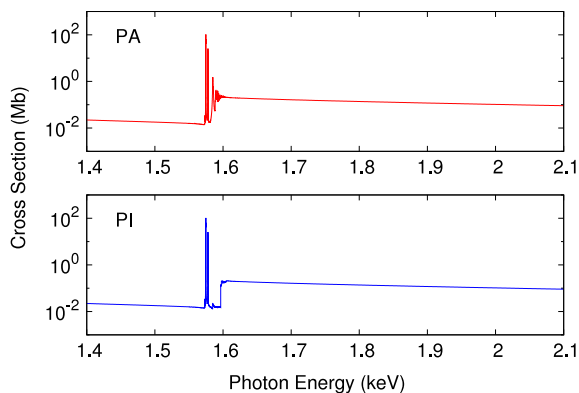


Fig. 9. Total photoabsorption (top) and photoionization (bottom) cross sections of Na-like Al. The photoionization cross section does not include the effect of spectator Auger loss.

background cross section from Verner and Yakovlev agree with the present results to within 10% at all energies.

We are in very good agreement with the previous Li-like calculation [15] with respect to the background cross section and resonance positions. However, since the spectator Auger process cannot occur for Li-like systems, there is no Auger damping and the associated broadening of the resonances converging to the K edge. Special effort must therefore be taken to ensure that all the resonances are properly resolved. This does not appear to be sufficiently done in the previous work [15] and we find large differences in the convolved cross sections. In Fig. 10, we compare

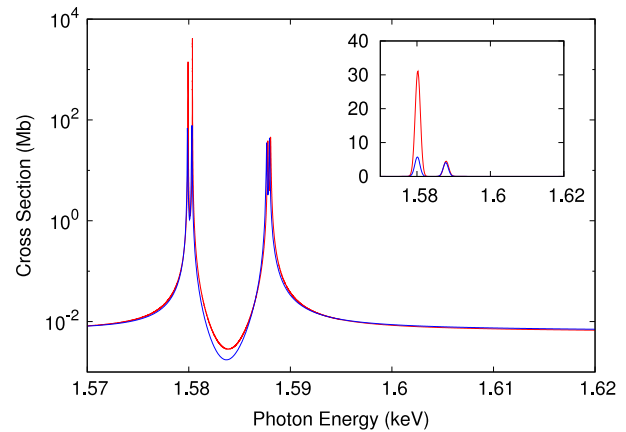


Fig. 10. Close-up of $K\alpha$ resonances from the Li-like Al total photoionization cross section. Comparison is made between the present calculations (red) and those from Ref. [15] (blue). Inset shows a convolution using a Gaussian with the width, $\Delta E/E = 10^{-3}$. (For interpretation of the references to colour in this figure legend, the reader is referred to the web version of this article.)

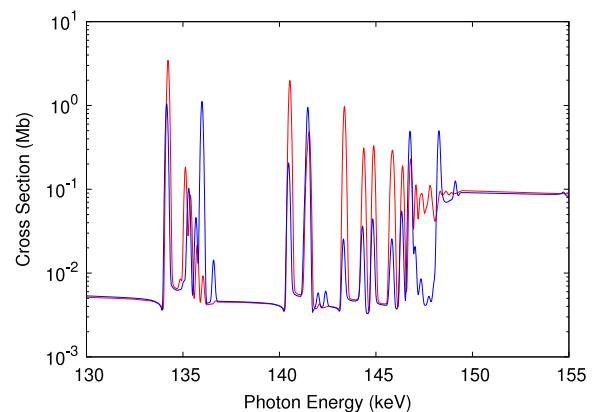


Fig. 11. Close-up of resonances near the K edge of the Li-like Al total photoionization cross section. The cross section has been convolved with a Gaussian with the width, $\Delta E/E = 10^{-3}$. Comparison is made between the present calculations (red) and those from Ref. [15] (blue). (For interpretation of the references to colour in this figure legend, the reader is referred to the web version of this article.)

the raw photoionization cross sections from the present work and Ref. [15] in the region of the $K\alpha$ resonances. In the inset of the figure are the convolved cross sections using a Gaussian with a width of $\Delta E/E = 10^{-3}$. The present results show the peak of the resonances near 1.58 keV to be nearly 100 times higher than those from the previous work. The impact on the convolved cross sections is an increase of more than a factor of 50. A lack of resolution can lead to resonances which can be too small or too large. This is seen in Fig. 11 where we compare convolved cross sections near the K edge. The previous calculation overestimates features by up to an order of magnitude in some places and underestimates features by up to two orders of magnitude at other energies. Overall, the present results show much more resonant enhancement, particularly near the K edge. These differences are entirely due to a lack of resonance resolution in the previous work.

A previous R -matrix calculation for photoionization of N-like Al was made by Zeng et al. [16]. Unfortunately, their data do not appear to be available electronically. In Fig. 12, we compare the present results for the $K\alpha$ resonance with the Zeng et al. results extracted manually from Fig. 1 in their work. This resonance is quite narrow in their figure, so we were only able to extract meaningful data near the base of the resonance. Their resonance peaks at over 10 MB where their Fig. 1 range cuts off. Despite the difficulty

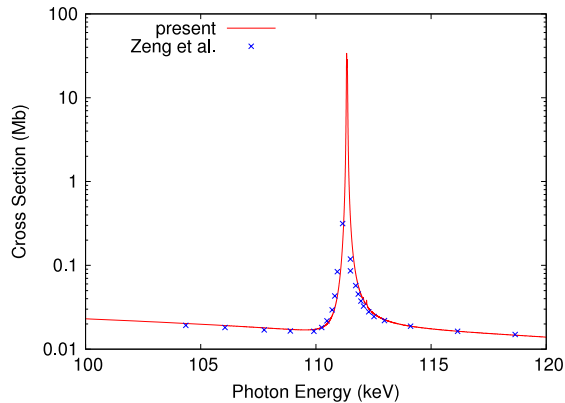


Fig. 12. Close-up of the $K\alpha$ resonance in the photoionization cross section for N-like Al. Comparison is made between the present calculation (red curve) and the results from Ref. [16] (blue crosses). Note that the results from Ref. [16] have been manually extracted from the Fig. 1 in their paper and subject to some uncertainty.

retrieving their results, the agreement between the two calculations is quite good. The background cross sections agree very well as does the width of the $K\alpha$ resonance. There may be a small shift in the resonance position, but this shift is well within the uncertainty of our calculation. We are unable to retrieve further resonance structure from the Zeng et al. figure due to its energy scale. The effects of radiative and Auger damping on the $K\alpha$ resonance is negligible, but this is not the case for resonances near the K edge. As it does not appear that Zeng et al. include damping in their calculations, we expect poorer agreement near the K edge. With no damping, their photoionization and photoabsorption cross sections are identical. Near the edge, our photoionization cross section will have smaller resonances than Zeng et al. and our resonances in the photoabsorption cross section will be broader, but should still agree with Zeng et al. in terms of total area. See Fig. 5 for the present cross sections.

As part of this paper, we provide electronic tables of the total photoabsorption cross sections and the total/partial cross sections for photoionization (as supplemental material posted in conjunction with the on-line version of the published manuscript). Note that the photoionization cross sections are missing the contribution from spectator Auger, which can be significant, but recoverable to a degree using the method discussed previously. In order to fully resolve all resonance features, particularly for Li-like Al, we use a large number of energy points. This amount of data can be cumbersome for plasma modeling codes, therefore we also provide cross sections which are convolved with a Gaussian having a width of $\Delta E/E = 10^{-4}$. This width is smaller than the spectral resolution of current and near-future detectors, so the effect of this broadening should be negligible on plasma models. In Figs. 13 and 14, we compare the raw, total photoabsorption cross section for Li-like Al with cross sections convolved with Gaussians of widths $\Delta E/E = 10^{-4}$ and 10^{-3} ; the latter width is representative of the resolution of current detectors. The first figure shows the $K\beta$ resonances while the second shows the K edge region.

As an example of the data to be found in the on-line archive, we show a table with convolved total photoionization cross sections for the ground state of Ne-like Al in Table .1.

4. Conclusions

Total photoabsorption and total/partial photoionization cross sections have been computed for the Li-like to Na-like ions of Al using the Breit–Pauli R -matrix method. These data will allow modelers of X-ray plasmas to identify Al features beyond the H-like and He-like systems.

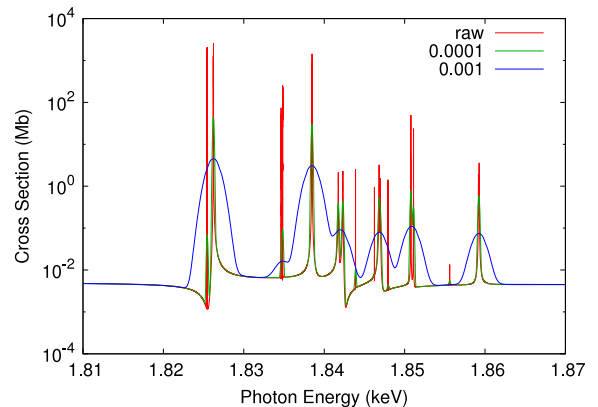


Fig. 13. Photoabsorption of Li-like Al in region around $K\beta$ resonance. Comparison of raw cross section (red) with convolution with a Gaussian having widths, $\Delta E/E = 0.0001$ (green) and $\Delta E/E = 0.001$ (blue). (For interpretation of the references to colour in this figure legend, the reader is referred to the web version of this article.)

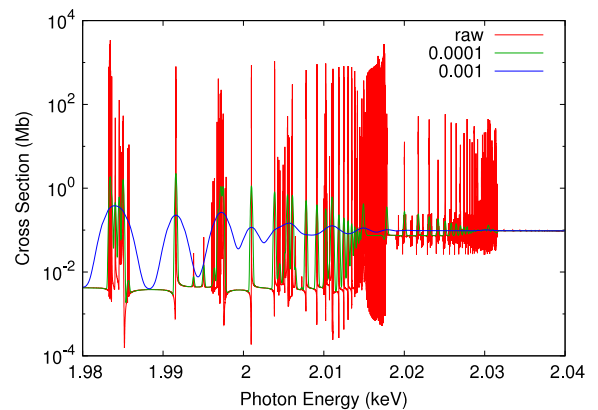


Fig. 14. Photoabsorption of Li-like Al in region around K edge. Comparison of raw cross section (red) with convolution with a Gaussian having widths, $\Delta E/E = 0.0001$ (green) and $\Delta E/E = 0.001$ (blue). (For interpretation of the references to colour in this figure legend, the reader is referred to the web version of this article.)

All data are included with this work as electronic tables. Both raw and convolved cross sections are available. A Gaussian convolution width of $\Delta E/E = 10^{-4}$ is used for the latter. The convolved data is also available in the xstar database² and the Universal Atomic Database (uadb).³

Acknowledgments

We would like to thank the referee whose suggestions helped improve the quality of this work. Support for this research was provided in part by a grant from the NASA Astronomy and Physics Research (APRA) program. PP and PQ are respectively Research Associate and Senior Research Associate of the Belgian F.R.S.-FNRS. Financial support from this organization is acknowledged. Computational time was awarded by the NASA Center for Climate Simulation (NCCS).

Appendix. Supplementary data

Supplementary material related to this article can be found online at <http://dx.doi.org/10.1016/j.adt.2012.04.003>.

² <http://heasarc.gsfc.nasa.gov/docs/software/xstar/xstar.html>.

³ <http://heasarc.gsfc.nasa.gov/uadb/>.

References

- [1] J. García, T.R. Kallman, M. Witthoef, E. Behar, C. Mendoza, P. Palmeri, P. Quinet, M.A. Bautista, M. Klapisch, *ApJS* 185 (2009) 477–485.
- [2] J. García, C. Mendoza, M.A. Bautista, T.W. Gorczyca, T.R. Kallman, P. Palmeri, *ApJS* 158 (2005) 68–79.
- [3] P. Palmeri, P. Quinet, C. Mendoza, M.A. Bautista, J. García, T.R. Kallman, *ApJS* 177 (2008) 408–416.
- [4] M.C. Witthoef, M.A. Bautista, C. Mendoza, T.R. Kallman, P. Palmeri, P. Quinet, *ApJS* 182 (2009) 127–130.
- [5] M.C. Witthoef, J. García, T.R. Kallman, M.A. Bautista, C. Mendoza, P. Palmeri, P. Quinet, *ApJS* 192 (2011) 7.
- [6] M.A. Bautista, C. Mendoza, T.R. Kallman, P. Palmeri, *A&A* 403 (2003) 339–355.
- [7] P. Palmeri, C. Mendoza, T.R. Kallman, M.A. Bautista, *A&A* 403 (2003) 1175–1184.
- [8] P. Palmeri, C. Mendoza, T.R. Kallman, M.A. Bautista, M. Meléndez, *A&A* 410 (2003) 359–364.
- [9] C. Mendoza, T.R. Kallman, M.A. Bautista, P. Palmeri, *A&A* 414 (2004) 377–388.
- [10] M.A. Bautista, C. Mendoza, T.R. Kallman, P. Palmeri, *A&A* 418 (2004) 1171–1178.
- [11] T.R. Kallman, P. Palmeri, M.A. Bautista, C. Mendoza, J.H. Krolik, *ApJS* 155 (2004) 675–701.
- [12] P. Palmeri, P. Quinet, C. Mendoza, M.A. Bautista, J. García, M.C. Witthoef, T.R. Kallman, *ApJS* 179 (2008) 542–552.
- [13] M.C. Witthoef, M.A. Bautista, J. García, T.R. Kallman, C. Mendoza, P. Palmeri, P. Quinet, *ApJS* 196 (2011) 7.
- [14] P. Palmeri, P. Quinet, C. Mendoza, M.A. Bautista, J. García, M.C. Witthoef, T.R. Kallman, *A&A* 525 (2011) A59+.
- [15] S.N. Nahar, *New Astron.* 13 (2008) 619–638.
- [16] J. Zeng, J. Yuan, Q. Lu, *Phys. Rev. A: At. Mol. Opt. Phys.* 64 (2001) 042704.
- [17] W.J. Veigele, *Atomic Data* 5 (1973) 51.
- [18] D.A. Verner, D.G. Yakovlev, *A&AS* 109 (1995) 125–133.
- [19] M.J. Seaton, *J. Physics B Atomic Molecular Physics* 20 (1987) 6363–6378.
- [20] J.A. Tully, M.J. Seaton, K.A. Berrington, *J. Physics B Atomic Molecular Physics* 23 (1990) 3811–3837.
- [21] J.A. Fernley, A. Hibbert, A.E. Kingston, M.J. Seaton, *J. Physics B Atomic Molecular Physics* 32 (1999) 5507–5522.
- [22] D. Luo, A.K. Pradhan, *J. Physics B Atomic Molecular Physics* 22 (1989) 3377–3395.
- [23] A. Hibbert, M.P. Scott, *J. Physics B Atomic Molecular Physics* 27 (1994) 1315–1323.
- [24] K.S. Baliyan, A.E. Kingston, *J. Physics B Atomic Molecular Physics* 24 (1991) 4743–4758.
- [25] S.N. Nahar, A.K. Pradhan, *Phys. Rev. A: At. Mol. Opt. Phys.* 45 (1992) 7887–7893.
- [26] J.B. West, T. Andersen, R.L. Brooks, F. Folkmann, H. Kjeldsen, H. Knudsen, *Phys. Rev. A: At. Mol. Opt. Phys.* 63 (2001) 052719–+.
- [27] C.E. Hudson, J.B. West, K.L. Bell, A. Aguilar, R.A. Phaneuf, F. Folkmann, H. Kjeldsen, J. Bozek, A.S. Schlachter, C. Cisneros, *J. Physics B Atomic Molecular Physics* 38 (2005) 2911–2932.
- [28] P.G. Burke, M.J. Seaton, *Numerical Solution of the Integro-Differential Equations of Electron-Atom Collision Theory*, in: *Methods in Computational Physics*, vol. 10, Academic Press, p. 1.
- [29] P.G. Burke, A. Hibbert, W.D. Robb, *J. Phys. B: At. Mol. Opt. Phys.* 4 (1971) 153–161.
- [30] K.A. Berrington, P.G. Burke, J.J. Chang, A.T. Chivers, W.D. Robb, K.T. Taylor, *Comput. Phys. Commun.* 8 (1974) 149–198.
- [31] K.A. Berrington, P.G. Burke, M. Le Dourneuf, W.D. Robb, K.T. Taylor, V. Ky Lan, *Comput. Phys. Commun.* 14 (1978) 367–412.
- [32] K.A. Berrington, P.G. Burke, K. Butler, M.J. Seaton, P.J. Storey, K.T. Taylor, Y. Yan, *J. Phys. B: At. Mol. Opt. Phys.* 20 (1987) 6379–6397.
- [33] F. Robicheaux, T.W. Gorczyca, M.S. Pindzola, N.R. Badnell, *Phys. Rev. A: At. Mol. Opt. Phys.* 52 (1995) 1319–1333.
- [34] T.W. Gorczyca, N.R. Badnell, *J. Phys. B: At. Mol. Opt. Phys.* 29 (1996) L283–L290.
- [35] T.W. Gorczyca, N.R. Badnell, *J. Phys. B: At. Mol. Opt. Phys.* 33 (2000) 2511–2523.
- [36] K.A. Berrington, W.B. Eissner, P.H. Norrington, *Comput. Phys. Commun.* 92 (1995) 290–420.
- [37] N.R. Badnell, *J. Phys. B: At. Mol. Opt. Phys.* 19 (1986) 3827–3835.
- [38] N.R. Badnell, *J. Phys. B: At. Mol. Opt. Phys.* 30 (1997) 1–11.
- [39] Y. Ralchenko, A.E. Kramida, J. Reader, NIST ASD Team, NIST Atomic Spectra Database (version 4.0), National Institute of Standards and Technology, Gaithersburg, MD, 2008. <http://physics.nist.gov/asd3>.

Explanation of Table**Table 1** **Example Table: total photoionization cross sections from the ground state of Ne-like Al convolved with a Gaussian of width $\Delta E/E = 10^{-4}$.**

This is an example of the tables included electronically as supplemental material with the on-line version of the published manuscript. The files are also available through the Universal Atomic Database (<http://heasarc.gsfc.nasa.gov/uadb/>)

Photon energy The photon energy in Rydbergs

Cross section The photoionization cross section in 10^6 barns

Table 1
Total photoionization cross sections from the ground state of Ne-like Al convolved with a Gaussian of width $\Delta E/E = 10^{-4}$.

Photon energy (Ry)	Cross section (MB)	Photon energy (Ry)	Cross section (MB)	Photon energy (Ry)	Cross section (MB)
8.8192799996E+00	3.638E+00	8.8543253940E+00	4.710E+00	8.9793774214E+00	5.781E+00
9.1393591046E+00	6.117E+00	9.2993407878E+00	1.346E+01	9.4593224710E+00	4.277E+00
9.6193041542E+00	4.516E+00	9.9394605020E+00	4.611E+00	1.0579387235E+01	4.530E+00
1.0739368918E+01	4.859E+00	1.0899350601E+01	4.027E+00	1.1219313968E+01	4.214E+00
1.1379295651E+01	3.811E+00	1.1539470316E+01	4.138E+00	1.1699451999E+01	4.103E+00
1.2019415365E+01	3.710E+00	1.2179397049E+01	3.804E+00	1.3139287148E+01	3.449E+00
1.3299461813E+01	3.302E+00	1.4579315278E+01	2.948E+00	1.4739296961E+01	3.007E+00
1.4899471626E+01	2.889E+00	1.5219434993E+01	2.489E+00	1.5379416676E+01	2.799E+00
1.5539398359E+01	2.617E+00	1.5699380042E+01	2.765E+00	1.5859361725E+01	2.457E+00
1.6019343409E+01	2.510E+00	1.6179325092E+01	2.390E+00	1.6339306775E+01	2.349E+00
1.6499288458E+01	2.371E+00	1.6659463123E+01	2.240E+00	1.6819444806E+01	2.250E+00
2.0339427800E+01	1.521E+00	2.0499409483E+01	1.520E+00	2.1779455930E+01	1.328E+00
2.4339355843E+01	1.038E+00	2.6899448737E+01	8.260E-01	2.9459348650E+01	6.670E-01
3.2019441545E+01	5.448E-01	3.4579341458E+01	4.505E-01	3.7139434352E+01	3.766E-01
3.9699334265E+01	3.175E-01	4.2259427159E+01	2.699E-01	4.4819327072E+01	2.313E-01
4.7379419967E+01	1.998E-01	4.9939319879E+01	1.735E-01	5.2499412774E+01	1.515E-01
5.5059312687E+01	1.331E-01	6.0179305494E+01	1.044E-01	6.5299298301E+01	8.313E-02
7.0419291108E+01	6.736E-02	7.5539283915E+01	5.524E-02	8.0659469704E+01	4.580E-02
8.5779462511E+01	3.847E-02	9.0899455318E+01	3.252E-02	9.6019948125E+01	2.770E-02
1.0113944093E+02	2.382E-02	1.0625943374E+02	2.052E-02	1.1137942654E+02	1.766E-02
1.1393932646E+02	1.660E-02	1.1461939335E+02	1.714E-02	1.1482414674E+02	1.795E-02
1.1492661993E+02	1.873E-02	1.152890014E+02	2.003E-02	1.1513137333E+02	2.241E-02
1.1518251343E+02	2.435E-02	1.1523384652E+02	2.721E-02	1.1528498662E+02	3.160E-02
1.1531065316E+02	3.475E-02	1.1533612673E+02	3.882E-02	1.1536179327E+02	4.431E-02
1.1538745981E+02	5.188E-02	1.1541293337E+02	6.262E-02	1.1542586313E+02	6.992E-02
1.1543859991E+02	7.882E-02	1.1545133669E+02	9.002E-02	1.1546426646E+02	1.046E-01
1.1547700324E+02	1.235E-01	1.1548974002E+02	1.488E-01	1.1550266978E+02	1.845E-01
1.1550903817E+02	2.074E-01	1.1551540656E+02	2.351E-01	1.1552177495E+02	2.693E-01
1.1552814334E+02	3.118E-01	1.1553451173E+02	3.656E-01	1.1554088012E+02	4.344E-01
1.1554744149E+02	5.262E-01	1.1555380988E+02	6.427E-01	1.1556017827E+02	7.982E-01
1.1556654666E+02	1.007E+00	1.1556982735E+02	1.142E+00	1.1557291505E+02	1.292E+00
1.1557619574E+02	1.479E+00	1.1558256413E+02	1.933E+00	1.1559530091E+02	3.116E+00
1.1559858160E+02	3.370E+00	1.1560186228E+02	3.538E+00	1.1560494999E+02	3.594E+00
1.1560823067E+02	3.534E+00	1.1561131838E+02	3.376E+00	1.1561768677E+02	2.843E+00
1.1562424814E+02	2.217E+00	1.1563061653E+02	1.695E+00	1.1563370423E+02	1.488E+00
1.1563698492E+02	1.298E+00	1.1564026561E+02	1.137E+00	1.1564663400E+02	8.923E-01
1.1565300239E+02	7.141E-01	1.1565937078E+02	5.825E-01	1.1566573917E+02	4.835E-01
1.1567210756E+02	4.077E-01	1.1567866893E+02	3.471E-01	1.1568503732E+02	3.004E-01
1.1569140571E+02	2.628E-01	1.1569777410E+02	2.322E-01	1.1571051088E+02	1.856E-01
1.1572344064E+02	1.522E-01	1.1573617742E+02	1.280E-01	1.1574891420E+02	1.098E-01
1.1576184397E+02	9.547E-02	1.1577458075E+02	8.437E-02	1.1578731753E+02	7.542E-02
1.1581298407E+02	6.202E-02	1.1583865061E+02	5.268E-02	1.1586412417E+02	4.596E-02
1.1588979072E+02	4.088E-02	1.1591545726E+02	3.699E-02	1.1596659736E+02	3.148E-02
1.1601773747E+02	2.783E-02	1.1606907055E+02	2.527E-02	1.1617135076E+02	2.199E-02
1.1627382395E+02	2.000E-02	1.1647857735E+02	1.765E-02	1.1678580393E+02	1.512E-02
1.1692648746E+02	1.313E-02	1.1693941722E+02	1.330E-02	1.1694578561E+02	1.368E-02
1.1695215401E+02	1.448E-02	1.1695852240E+02	1.611E-02	1.1696180308E+02	1.751E-02
1.1696489079E+02	1.939E-02	1.1696817147E+02	2.220E-02	1.1697145216E+02	2.614E-02
1.1697453986E+02	3.117E-02	1.1697782055E+02	3.804E-02	1.1698746962E+02	6.222E-02
1.1699055733E+02	6.728E-02	1.1699383801E+02	6.928E-02	1.1699692572E+02	6.799E-02
1.1700329411E+02	5.926E-02	1.1700985548E+02	4.881E-02	1.1701622387E+02	4.100E-02
1.1702259226E+02	3.556E-02	1.1702896065E+02	3.179E-02	1.1703532904E+02	2.911E-02
1.1704825880E+02	2.556E-02	1.1706099558E+02	2.344E-02	1.1708666213E+02	2.099E-02
1.1711213569E+02	1.965E-02	1.1716346877E+02	1.816E-02	1.1741936227E+02	1.488E-02
1.1748343214E+02	1.341E-02	1.1748980053E+02	1.377E-02	1.1749288823E+02	1.424E-02
1.1749616892E+02	1.506E-02	1.1749944961E+02	1.632E-02	1.1751218639E+02	2.353E-02
1.1751546707E+02	2.463E-02	1.1751855478E+02	2.503E-02	1.1752492317E+02	2.439E-02
1.1753785293E+02	2.163E-02	1.1755058971E+02	1.983E-02	1.1756332649E+02	1.875E-02
1.1758899303E+02	1.756E-02	1.1769146622E+02	1.552E-02	1.1774260633E+02	1.427E-02
1.1775534311E+02	1.428E-02	1.1776171150E+02	1.500E-02	1.1777464126E+02	1.826E-02
1.1778100965E+02	1.911E-02	1.1778737804E+02	1.903E-02	1.1781304458E+02	1.728E-02
1.1790258801E+02	1.475E-02	1.1790895640E+02	1.487E-02	1.1791532479E+02	1.543E-02
1.1792825455E+02	1.716E-02	1.1793462294E+02	1.736E-02	1.1798576305E+02	1.547E-02
1.1800506120E+02	1.524E-02	1.1802416637E+02	1.652E-02	1.1806256969E+02	1.547E-02
1.1808823624E+02	1.614E-02	1.1811370980E+02	1.563E-02	1.1812663956E+02	1.588E-02
1.1828025285E+02	1.573E-02	1.1828334056E+02	1.593E-02	1.1828488441E+02	1.631E-02
1.1828662124E+02	1.733E-02	1.1828816509E+02	1.928E-02	1.1828970895E+02	2.295E-02
1.1829144578E+02	3.021E-02	1.1829298963E+02	4.041E-02	1.1829453348E+02	5.466E-02
1.1829627032E+02	7.528E-02	1.1830090187E+02	1.396E-01	1.1830263871E+02	1.596E-01
1.1830418256E+02	1.733E-01	1.1830572641E+02	1.830E-01	1.1830900710E+02	1.931E-01
1.1871851389E+02	1.943E-01	1.2129944879E+02	1.809E-01	1.2292975670E+02	1.758E-01
1.2294249348E+02	1.797E-01	1.2294905486E+02	1.858E-01	1.2296179164E+02	1.765E-01
1.2337129843E+02	1.752E-01	1.2380666475E+02	1.813E-01	1.2383850670E+02	1.881E-01
1.2384506807E+02	1.853E-01	1.2386417324E+02	1.602E-01	1.2387054163E+02	1.604E-01

(continued on next page)

Table 1 (continued)

Photon energy (Ry)	Cross section (MB)	Photon energy (Ry)	Cross section (MB)	Photon energy (Ry)	Cross section (MB)
1.2388347139E+02	1.678E-01	1.2393461150E+02	1.755E-01	1.2403689171E+02	1.822E-01
1.2408822479E+02	1.896E-01	1.2411369835E+02	1.991E-01	1.2412025972E+02	1.946E-01
1.2412662811E+02	1.849E-01	1.2413299650E+02	1.819E-01	1.2417139983E+02	2.066E-01
1.2418413661E+02	2.205E-01	1.2419706637E+02	2.451E-01	1.2420980315E+02	2.779E-01
1.2421289086E+02	2.737E-01	1.2421617154E+02	2.533E-01	1.2421945223E+02	2.147E-01
1.2422582062E+02	1.210E-01	1.2422736447E+02	1.033E-01	1.2422890832E+02	8.961E-02
1.2423064516E+02	7.901E-02	1.2423218901E+02	7.353E-02	1.2423373286E+02	7.115E-02
1.2423546969E+02	7.126E-02	1.2423855740E+02	7.594E-02	1.2425129418E+02	1.045E-01
1.2425785555E+02	1.151E-01	1.2427059233E+02	1.287E-01	1.2429625887E+02	1.428E-01
1.2434739898E+02	1.543E-01	1.2444987217E+02	1.646E-01	1.2450101227E+02	1.724E-01
1.2451374905E+02	1.769E-01	1.2452648583E+02	1.851E-01	1.2454250330E+02	2.068E-01
1.2454578398E+02	2.053E-01	1.2454906467E+02	1.944E-01	1.2455543306E+02	1.518E-01
1.2455852076E+02	1.343E-01	1.2456180145E+02	1.252E-01	1.2456488915E+02	1.244E-01
1.2457781892E+02	1.394E-01	1.2459055570E+02	1.476E-01	1.2461622224E+02	1.546E-01
1.2471850245E+02	1.676E-01	1.2473143221E+02	1.719E-01	1.2474416899E+02	1.799E-01
1.2475053738E+02	1.810E-01	1.2475381807E+02	1.762E-01	1.2476346714E+02	1.450E-01
1.2476655485E+02	1.392E-01	1.2476983553E+02	1.377E-01	1.2479530909E+02	1.508E-01
1.2484664218E+02	1.573E-01	1.2542249905E+02	1.691E-01	1.2543542881E+02	1.637E-01
1.2544816559E+02	1.451E-01	1.2545453398E+02	1.411E-01	1.2548020052E+02	1.527E-01
1.2558248073E+02	1.616E-01	1.2576176057E+02	1.690E-01	1.2578742711E+02	1.592E-01
1.2583856721E+02	1.648E-01	1.2586423375E+02	1.647E-01	1.2596651396E+02	1.792E-01
1.2597944372E+02	1.780E-01	1.2599218050E+02	1.807E-01	1.2601128568E+02	1.934E-01
1.2601784705E+02	1.917E-01	1.2602093475E+02	1.864E-01	1.2602421544E+02	1.762E-01
1.2603386451E+02	1.296E-01	1.2603695222E+02	1.181E-01	1.2604023290E+02	1.110E-01
1.2604332061E+02	1.090E-01	1.2604968900E+02	1.132E-01	1.2606261876E+02	1.275E-01
1.2608809232E+02	1.389E-01	1.2613942541E+02	1.487E-01	1.2621623205E+02	1.563E-01
1.2626737216E+02	1.544E-01	1.2633144202E+02	1.604E-01	1.2635691558E+02	1.554E-01
1.2638258213E+02	1.571E-01	1.2640824867E+02	1.546E-01	1.2651052888E+02	1.627E-01
1.2656186196E+02	1.701E-01	1.2657459874E+02	1.666E-01	1.2658733552E+02	1.499E-01
1.2659370391E+02	1.449E-01	1.2663210724E+02	1.521E-01	1.2665777378E+02	1.483E-01
1.2684342201E+02	1.654E-01	1.2686252718E+02	1.484E-01	1.2687545694E+02	1.471E-01
1.2700340369E+02	1.602E-01	1.2701614047E+02	1.513E-01	1.2702907023E+02	1.489E-01
1.2709294712E+02	1.581E-01	1.2711861366E+02	1.505E-01	1.2716975376E+02	1.553E-01
1.2718249054E+02	1.528E-01	1.2720815709E+02	1.558E-01	1.2738743692E+02	1.541E-01
1.2741291048E+02	1.601E-01	1.3441929768E+02	1.344E-01	1.3953929049E+02	1.210E-01
1.4977946909E+02	1.004E-01	1.6001945470E+02	8.448E-02	1.7025944032E+02	7.173E-02
1.8049942593E+02	6.148E-02	1.9073941155E+02	5.316E-02	2.0097939716E+02	4.617E-02
2.1121938278E+02	4.032E-02	2.2353932326E+02	3.462E-02		